IEEE Access
Multidisciplinary | Rapid Review | Open Access Journal

Received 1 March 2026, accepted 24 March 2026, date of publication 2 April 2026, date of current version 7 April 2026.

Digital Object Identifier 10.1109/ACCESS.2026.3680166

RESEARCH ARTICLE

Camera Noise Extraction From a Raw Single Image by Segmentation, Multiple Approximations, and Weighted Averaging

ALEXANDER V. KOZLOV, PAVEL A. CHEREMKHIN, ANTON A. VOLKOV, ANDREY S. SVISTUNOV, ROSTISLAV S. STARIKOV, VSEVOLOD A. NEBAVSKIY, EVGENII YU. ZLOKAZOV, AND VLADISLAV G. RODIN

National Research Nuclear University MEPhI (Moscow Engineering Physics Institute), 115409 Moscow, Russia

Corresponding author: Pavel A. Cheremkhin (CheremhinPavel@mail.ru)

This work was supported by the Russian Science Foundation (RSF) under Grant 24-19-00898.

ABSTRACT Digital cameras are widely used in a variety of applications, including medicine, security, material characterization, and metrology. To reduce cost, increase dynamic range, and minimize noise, accurate knowledge of camera parameters, including noise characteristics, is required. The most promising camera noise estimation methods use a single image. However, most methods estimate the noise of the acquired image rather than the intrinsic sensor noise of the camera. In this paper, a method is proposed to estimate main noise components from a single image: light temporal, light spatial and dark noise. The method is based on segmentation, multi-interval approximation, and weighted averaging. The method was experimentally validated on a dataset obtained from a camera whose noise parameters were independently measured. The noise estimation error was reduced to single-digit or several tens of percent, which is more than 5 times better than using patch-based approximation. The proposed method can be used in signal and image processing, for camera selection, noise reduction, image authenticity, and so on.

INDEX TERMS Noise estimation, sensor, image segmentation, multi-parameter approximation, weighted averaging, noise level, photo-response non-uniformity, sensor, shot noise, uncertainty measurement.

I. INTRODUCTION

Today, digital cameras are used in a wide range of applications [1]: medicine [2], [3], biology [4], [5], 3D detection [6], [7], multispectral imaging [8], nondestructive testing [9], person re-identification [10], gaze direction [11], object tracking [12], vehicle counting [13], science [14], and others [15]. For each application, specific characteristics are important, including technical parameters (dimensions, pixel count, bit depth), noise properties, and spectral and radiometric characteristics [16]. At the same time, manufacturers often do not specify some characteristics, including camera noise [17] and correct dynamic range values [18]. Noise affects the resolution of optical-digital systems [19] and negatively affects their calibration [20]. Noise can be increased due to acquiring certain data algorithms [21], corrupted data [22], and low-light conditions [23]. To reduce noise, a digital camera should be chosen for a required task and algorithms should be used to increase image quality [24], [25], [26]. The most effective algorithms require the introduction of a value describing the signal deviation [27], like in BM3D [28]. This deviation value can be calculated on the basis of the camera sensor noise. Noise characteristics of existing devices across different classes can be used for modeling [29], [30], [31], [32] and checking the stability of optoelectronic systems to noise, generating data sets [33], understanding latent correspondences across modalities [34], training neural networks [25], [30], [35], including autoexposure [36], low-light photography [31], synthetic noise extraction [37] and correction of the photon transfer function [38].

Noise in digital camera sensors is classified into dark and light components, and into temporal and spatial components.

The associate editor coordinating the review of this manuscript and approving it for publication was Joewono Widjaja.

[39]. Light noise appears only in the presence of a signal, while dark noise exists even in the absence of a signal. Spatial noise is constant in time [40] and forms unique portraits due to small differences in pixel sensitivity, while temporal noise varies from frame to frame. In order to provide fast and reliable measurements of digital camera noise, many methods have been developed that require different numbers of images. The most accurate methods are specified in the European Machine Vision Association (EMVA) 1288 Standard [39]. However, its realization requires the use of a uniform scene and at least 50 series of images at different brightness levels containing 2 frames each. The application of this method is time-consuming and requires a special experimental setup [41].

Therefore, methods based on automatic scene segmentation have been developed to simplify and speed up the estimation of camera noise characteristics [42], [43], [44], [45], [46], [47]. The methods used different scenes: uniform [43], nonuniform [44], [45], [46], and strip [47]. The required number of frames is 4 for the uniform scene method [43], 2 for the nonuniform [44], [45], and strip [47], and one for denoising [46]. The execution time and requirements for experimental setup are significantly reduced [42]. However, noise estimation requires recording of a special scene frames.

The next step in the development of noise estimation methods is the evaluation of all noise components from a single frame of an arbitrary scene. There are methods that estimate noise from a single frame [46], [48], [49], [50], [51], [52], [53], [54], [55], [56], [57], [58], [59], [60], [61], [62], [63], [64]. However, they are essentially designed to estimate the noise of an image rather than the camera noise. Therefore, these methods typically provide only an upper bound of the noise level [51]. Since the result of these algorithms is the dependence of the signal deviation on the signal level, it is not possible to separate the noise into temporal and spatial light and dark components.

Another group of methods is deep learning-based approaches [20], [31], [32], [65], [66], [67], [68], [69], [70], [71], [72]. These methods require extensive training on datasets containing either clean or noisy images. While typically designed for image denoising tasks, these networks often focus on estimating the composite image noise rather than strictly isolating the underlying camera sensor noise [73]. However, photo response non-uniformity (PRNU) remains challenging to extract, with some models treating pixel responses as spatially constant [74].

Thus, the aim of this work is to develop an approach that allows to estimate individually the noise characteristics of a camera sensor from a single image. It uses the obtained dependence of noise on signal level, grouping of points of these dependencies and approximation for each type of noise. The main contributions can be formulated as follows:

1. The proposed method estimates total noise value from a single image. For the first time, the results were successfully verified in optical experiments and compared with the noise measurement by the EMVA 1288 Standard.

2. For the first time, the method estimates main noise component 'parameters according to the EMVA 1288 Standard [39] from a single image: light temporal, light spatial and dark noise.

3. For the first time, PRNU value is correctly estimated from a single nonuniform image. Previously PRNU value was estimated from nonuniform multiple images in [75]. However, a) the method of [75] used multiple images, and b) these images were significantly homogeneous (non-uniformity was less than 20% of the signal).

4. For the first time, a dataset with experimentally measured sensor noise parameters according to standard specifications has been established. Existing publicly available image databases [76], [77], [78], [79], [80] lack rigorously validated noise characterization; typically, camera noise can only be approximated based on empirical relationships [81], which do not reflect actual sensor noise values. Although dedicated datasets exist for estimating noise in both synthesized [82] and real [83] camera images, they generally do not provide natural images suitable for rapid noise parameter estimation.

The paper is organized as follows. Section II describes camera noise and existing techniques for measuring it. Section III describes the proposed method for obtaining individual noise components. Section IV gives experimental validation results and comparison with patch-based approximation of data. Section V discusses the obtained data and the method features. The main results are given in the Conclusion.

II. RELATED WORKS

A. NOISE CLASSIFICATION

The currently widely used classification of noise is presented in the EMVA 1288 Standard [39]. Noises of digital cameras are divided into four subgroups: light temporal, dark temporal, light spatial and dark spatial. Light temporal noise appears when there is a light signal in a pixel and dark temporal noise appears when there is even no signal in a pixel. Temporal noises are not deterministic and take different values at each moment of time. Spatial noise does not change in time, as it is determined by the differences of pixels from each other and other features of the sensor. Light temporal noise corresponds to shot noise and is well described by the Poisson distribution [84]. It is characterized by the conversion gain K (digital numbers (DN) to charges conversion coefficient) [84]. The gain K relates the number of charges generated during the exposure in a pixel cell and the digital signal in a frame. For the entire sensor the average value of K is estimated [85]. The variance of light temporal noise is proportional to the signal level and is determined by the conversion gain, light temporal noise is expressed as number of charges. Dark temporal noise arises from thermally generated charges, dark current fluctuations, and other stochastic

processes. Its deviation is characterized by a single value in digital units. Light spatial noise is generated first of all due to small differences in the sensitive part of a pixel (fill-factor). It is characterized by photo response non-uniformity (PRNU), expressed in fractions or in percent. The deviation of light spatial noise is calculated as the product of PRNU by the signal in DN. Dark spatial noise is characterized by dark signal non-uniformity (DSNU). The deviation of dark spatial noise is expressed by the DSNU value in DN.

The total noise of a digital camera is described by the following equation:

$$\sigma_{tot}(S) = \sqrt{\sigma_{TN}^2 + \sigma_{SN}^2} = \sqrt{\sigma_{LTN}^2 + \sigma_{DTN}^2 + \sigma_{LSN}^2 + \sigma_{DSN}^2} = \sqrt{S \cdot K + \sigma_{DTN}^2 + (S \cdot PRNU)^2 + DSNU^2} \quad (1)$$

where $\sigma_{tot}(S)$ – total, σ_{TN} – temporal, σ_{SN} – spatial, σ_{LTN} – light temporal, σ_{DTN} – dark temporal, σ_{LSN} – light spatial and σ_{DSN} – dark spatial noises, S – signal value. Sometimes the uncertainty of analog-to-digital conversion [86] is considered separately. It is called quantization noise and it's standard deviation is equal to:

$$\sigma_{quant} = \frac{1}{\sqrt{12}} DN \approx 0.29 DN \quad (2)$$

B. NOISE MEASUREMENT ACCORDING TO THE EMVA 1288 STANDARD

According to the EMVA 1288 Standard it is suggested to record 50 series of uniform frames. Minimally each series of images contains 2 images. It is necessary that the average signal of the series of frames should be equidistantly distributed over the camera dynamic range, and it is obligatory to have a dark series of frames and a series at the average signal level. To increase the homogeneity of scenes, additional algorithms are used to avoid shading and vignetting [87].

The main stages of noise measurement in accordance with the EMVA 1288 Standard are shown in Fig. 1.

After recording all image series, (3-6) are used to calculate the noises:

$$\sigma_{DTN}^2 = E\left\{Var\{D\}_t\right\}_{xy} \quad (3)$$

$$DSNU^2 = Var\left\{E\{D\}_t\right\}_{xy} - \sigma_{DTN}^2 \quad (4)$$

$$\sigma_{LTN}^2 = E\left\{Var\{L\}_t\right\}_{xy} - \sigma_{DTN}^2 \quad (5)$$

$$PRNU = \frac{\sqrt{Var\left\{E\{L\}_t\right\}_{xy} - \sigma_{DTN}^2 - DSNU^2 - \sigma_{DTN}^2}}{E\{S\}_{xy} - E\{D\}_{xy}} \quad (6)$$

where $E\{\dots\}_j$ and $Var\{\dots\}_j$ – expectation and variance operators, j is coordinates of the analyzed region, x and y are coordinates of the image, t is the image number (time coordinate), D is a set of t dark images (3D array with x, y and t coordinates [88]), L – a set of t light images (3D array with x, y and t coordinates).

To estimate the gain K, the dependence of the temporal noise on the signal level is plotted according to (3,5) and

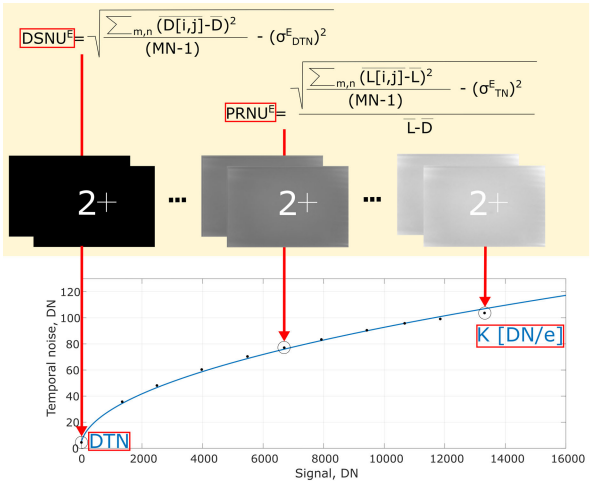

FIGURE 1. Measurement of camera noise according to the EMVA 1288 Standard.

approximated curve provides $\sqrt{S \cdot K}$ value for light temporal noise (see (1)).

Using a data set of one hundred (or more) images, all the noise components of digital cameras can be obtained. The standard provides highly accurate estimates but is labor-intensive and time-consuming. This leads even to the development of special hardware and software equipment for its realization [41].

C. NOISE ESTIMATION BY AUTOMATIC SCENE SEGMENTATION

Automatic segmentation is the process of sorting signals and signal deviations between frames, calculated based on at least two images of a single scene [42]. Automatic segmentation methods rely on a predetermined scene composition, which can be a gradient image, stripes and rings of varying brightness, uniform distribution, and etc. The methods used different scenes: uniform [43], nonuniform [44], [45], [46], and strip [47]. The required number of frames is four for the uniform scene method [43], two for the nonuniform [44], [45], and strip [47], and one for denoising [46]. The execution time and requirements for experimental setup are significantly reduced [42].

The most accurate method uses automatic segmentation of registered uniform scene [43]. It allows for the evaluation of all four sensor noise characteristics, as well as PRNU and DSNU matrices. A stripe scene [47] allows all four noise components evaluation based on a smaller number of images. The method based on automatic segmentation of a non-uniform scene [45] is the simplest and fastest to implement; however, it only allows for the temporal noise evaluation.

Depending on the task, one method or another may be preferable.

D. SINGLE-IMAGE NOISE ESTIMATION

Single-image noise estimation methods can be divided into three groups based on their operating principles: filtering-based, wavelet-based, and patch-based.

Filtering-based methods [52], [53], [54], [55] are the least complex. Noise is estimated by subtracting the filtered image from the original one and removing edges in the obtained image. The effectiveness of the method depends on the quality of filtering and edge removal algorithms. However, both algorithms depend strongly on parameter selection and also have their own imperfections. Therefore, developing a reliable filtering-based noise estimation algorithm is an extremely challenging task.

A slightly more complex approach is based on the wavelet transform. The resulting wavelet coefficients are used to estimate noise [46], [48], [56], [57]. However, as in the filtering-based approach, residual image boundaries significantly degrade the reliability of noise estimation. To eliminate their influence, edge removal, as in filtering-based methods, was additionally used in [48]. In [57], a threshold value was added, above which signals were removed from further analysis.

The patch approach [49], [50], [51], [58], [59], [60], [61], [62], [63], [64] has proven to be the most promising. The image is divided into separate groups of pixels, within which signal changes ideally occur only due to the presence of noise. Such a group of pixels is called a patch. In [58] and [59], the most uniform patches were identified by a threshold selection and were then analyzed using principle component analysis. In [61] and [64], noise was estimated by the calculation of the covariance matrix eigenvalues in redundant dimensions. In [64], images with additional noise were synthesized also, and the noise was estimated by averaging over several images in redundant dimensions.

The single-image methods are essentially designed to estimate the noise of an image rather than the registering camera noise. Therefore, usually an upper bound of the noise level is estimated [51]. Since the result of these algorithms is the dependence of the signal deviation on the signal level, it is not possible to separate the noise into temporal and spatial light and dark components.

It should be emphasized that most filtering-, wavelet-, patch-, and deep learning–based single-image noise estimation methods provide either (i) a global noise level, (ii) a signal-dependent variance curve typically fitted by a Poisson–Gaussian model, or (iii) pixel-wise variance maps. These outputs correspond to composite image noise and do not explicitly separate the contributions of light temporal, dark temporal, light spatial (*PRNU*), and dark spatial (*DSNU*) components as defined in the EMVA 1288 Standard. Consequently, a direct quantitative comparison in terms of EMVA parameters (*PRNU*, *K*, and *dark noise*) is generally not possible without additional model assumptions and reformulation.

E. DEEP-LEARNING BASED NOISE ESTIMATION

Recent progress in deep-learning has enabled the estimation of image noise parameters from a single image [20], [31], [32], [65], [66], [67], [68], [69], [70], [71], [72], overcoming several limitations of traditional methods that require specialized scenes or extensive acquisition protocols.

A seminal model, Deep Residual Noise Estimator (DRNE), utilizes a 16-layer convolutional structure with no pooling to preserve spatial information and outputs pixel-wise variance maps. DRNE achieves fine-grained noise estimation but is computationally intensive—processing a 500×500 image in 1.16s on GPU—and exhibits limited generalization due to exclusive training on synthetic homogeneous noise [66]. FADNet introduces frequency-domain attention, combining spatial features and multi-scale frequency cues to achieve notable efficiency and accuracy; it processes 512×512 images twice as fast as CycleISP and five times as fast as MPRNet, with a compact architecture (22M parameters, ≈88MB) [67], [89], [90]. However, both methods remain significantly more demanding than classical approaches.

Further advancements leverage physics-based models and contrastive learning (e.g., [32], [68],), employing architectures such as ResNet to disentangle signal-dependent and independent noise components, including spatially-structured noise. While comprehensive, these methods are often tailored to specific sensor types (e.g., Bayer CFA), with practical deployment hindered by high computational requirements [32], [68], [72], [91] and first of all aimed to denoise.

To address speed and resource constraints, lightweight convolutional regressors like PGE-Net have emerged, using input transformations such as the Generalized Anscombe Transform to stabilize noise statistics. PGE-Net often estimate noise parameter with reduced generality [46], [49], [69]. Transformer-based solutions, such as Condformer with Locally Noise Prior Estimation (LoNPE), embed noise priors into self-attention modules, achieving higher accuracy but incurring substantial memory and computational overhead (27M parameters, 565 GFLOPs, 3.8GB GPU memory) [92], [93].

The deep learning-based methods are typically designed for image denoising tasks, and focus on estimating the composite image noise rather than strictly isolating the underlying camera sensor noise [73]. However, separation of noises, photo response non-uniformity (PRNU) estimation and accurate total noise value remains very challenging to extract, with some models treating pixel responses as spatially constant [74].

F. IMAGE DATASETS

Validation in single-image noise estimation is critically dependent on datasets with known or unknown estimated noise characteristics. Two main categories exist: synthetic [76], [77], [78], [82] benchmarks, and real-world [79], [80], [81], [82] datasets.

Synthetic sets using BSD [76], McMaster [77], or USC-SIPI [78] offer ground-truth-established images but lack real sensor artifacts, and their parametric models usually do not capture complex real-world noise patterns.

Real-world datasets serve as operational benchmarks. The Smartphone Image Denoising Dataset (SIDD) provides ≈30,000 noisy and reference image pairs obtained through multi-frame averaging on five smartphone models, covering varied ISO and lighting, though it lacks explicit per-pixel noise decomposition [79]. The Darmstadt Noise Dataset (DND) [80] focuses on diverse consumer cameras and sensor sizes, employing paired high- and low-ISO acquisitions to derive reference images; however, separate EMVA 1288 component values must be estimated retrospectively. The Natural Image Noise Dataset (NED2012) offers ''experimentally measured'' noise curves but only for global two-parameter Poisson–Gaussian models, making it insufficient for separating all fundamental components [81]. Specialized datasets (e.g., CRVD [94], PMRID for video [95]; ELD [74] for low-light; HDR for high-dynamic-range) provide test cases for challenging and specific use scenarios.

Fundamentally, no available real-world dataset supplies direct ground truth for all four noise components according to the EMVA 1288 Standard [39]. The synthetic [82] and experimental [83] datasets with accurately estimated noises according to the EMVA 1288 Standard do not contain synthetic or natural amateur images. Most sets require post-processing and incur additional uncertainties in both extraction and evaluation [79], [80], [81]. High-fidelity PRNU value validation is unavailable due to practical challenges in data acquisition.

III. PROPOSED MODIFICATION FOR OBTAINING NOISE VS SIGNAL DEPENDENCY

There are methods of noise estimation using a single image [46], [48], [49], [50], [51], [52], [53], [54], [55], [56], [57], [58], [59], [60], [61], [62], [63], [64]. However, they do not provide a consistent signal–noise dependency in which each signal level corresponds to a unique noise value. Usually they provide set of points or an upper bound of the noise level [51]. This plot is required for estimation of noise parameters of digital cameras according to the EMVA 1288 Standard [39]. Therefore, it is necessary to transform all the obtained values to single standard output parameters. To satisfy these conditions, firstly we proposed modification of single-image noise estimation method.

A. THE PROPOSED MODIFICATION FOR OBTAINING NOISE VS SIGNAL DEPENDENCY (THE METHOD'S 1ST STAGE)

The original method of O. Laligant et al. [50] estimate camera noise from a single image. It is effective and simple patch-based method. The signal is represented in the form:

$$I_n = IH + n \tag{7}$$

where I is the signal amplitude in a pixel, H is the Heaviside function, n is the noise realization, which corresponds to the probability density function P_{Nk}, P_{Nk} is the probability density function of the noise distribution N_k. Polarized derivatives are calculated for noise estimation:

$$\begin{aligned}
\sigma_k^{R+} &= T\left(I_{n_{k+1}} - I_{n_k}\right) \\
\sigma_k^{R-} &= -T\left[-\left(I_{n_{k+1}} - I_{n_k}\right)\right] \\
\sigma_k^{L+} &= T\left(I_{n_k} - I_{n_{k-1}}\right) \\
\sigma_k^{L-} &= -T\left[-\left(I_{n_k} - I_{n_{k-1}}\right)\right]
\end{aligned} \tag{8}$$

where T is a nonlinear threshold operator, $T(u) = u$ when $u \geq 0$, and $T(u) = 0$ otherwise.

Further, the process of obtaining the estimate differs from the original method of O. Laligant et al. The aim of the changes is to obtain an estimate of the dependence of noise on signal level. The original method of O. Laligant involves estimating the image noise. In the proposed modified O. Laligant method, the noise is estimated as follows:

$$Noise_k = \sqrt{\frac{\left(\sigma_k^{R+}\right)^2 + \left(\sigma_k^{R-}\right)^2 + \left(\sigma_k^{L+}\right)^2 + \left(\sigma_k^{L-}\right)^2}{4}} \tag{9}$$

This formulation ensures robust noise estimation by incorporating all available data while suppressing local extrema. Median filter with a 3×3 window is applied to the registered image to obtain the signal value.

In order to represent the data in a form where one signal level corresponds to one noise level, we apply segmentation. It consists in grouping signals with a certain step. Each signal corresponds to one deviation. In order to estimate the signal value for a given step, we find the average values of all the signals in the segmentation step. The noise variance is computed as the mean squared deviation within each segment. Noise is the square root of this variance. The main steps of the modified method of O. Laligant are shown in Fig. 2.

Since the obtained noise–signal dependency serves as the input for all subsequent stages, its accuracy directly affects the final estimates of PRNU, gain K, and dark noise. Significant distortions at this stage (e.g., due to highly heterogeneous scenes or strong deviation from the assumed signal-dependent model) inevitably propagate to the final parameters. Therefore, the reliability of the first stage is a necessary condition for accurate EMVA-oriented decomposition.

B. THE PROPOSED METHOD FOR CAMERA NOISE COMPONENTS ESTIMATION (THE METHOD'S 2ND-9TH STAGE)

The proposed modification of the O. Laligant method provides the dependency of noise on the signal level from a single image. This dependency is a 1st stage of the main proposed method and is a basis for extracting the individual components of camera noise: light temporal, light spatial, and dark noise. The whole process of obtaining noise parameters from signals and the corresponding deviations consists of the 9 stages:

1. Application of proposed modification of the O. Laligant method.

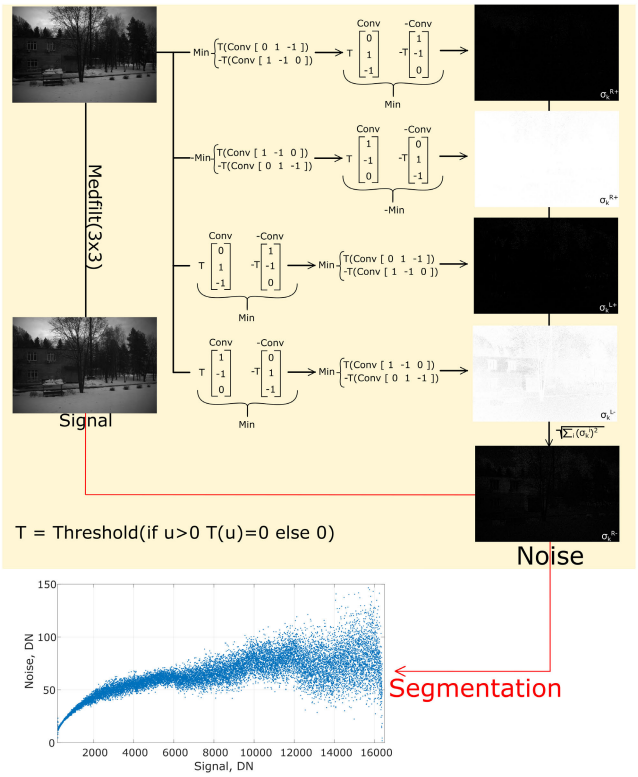

FIGURE 2. Scheme of the proposed modification of the O. Laligant method.

2. Readout of the signal array and deviation array from the noise vs signal dependency.
3. Removal of data containing signals less than 10% of the maximum and more than 90% of the maximum. The exclusion of low- and high-signal regions is introduced to suppress systematic distortions of the noise–signal dependency. At low signal levels, the number of available samples is often insufficient for statistically stable estimation, leading to high variance. At high signal levels, sensor saturation and nonlinear response violate the square-root behavior assumed by the EMVA-based model. Retaining these regions significantly degrades parameter stability. Therefore, signals below 10% and above 90% of the dynamic range are excluded to ensure physically consistent approximation.
4. Partitioning of the obtained noise dependence on the signal level into sections:
   a. Finding the difference of the minimum and maximum signals.
   b. Counting the number of unique signal levels between minimum and maximum signal. This allows select an adequate number of noise vs signal dependency steps on further method stages, taking into account estimated bit depth of the camera. For modern digital cameras with standard dynamic range the reasonable number of the dependency steps is from 10 to 100.
   c. Selecting the number of segmentation steps in the range of 10 to 100.
   d. Calculation of step St_1 for dividing the dependence of noise on signal level. Step St_1 is determined by dividing the difference of the minimum and maximum signals by the number obtained in stage 4c.
5. Using the data points separated by the intervals *In1*, calculated in stage 4.4 as the centers of the new small intervals In_2. The new small step St_2 for the intervals In_2 is equal to the half of that one obtained in stage 4d. Shifting the smaller intervals In_2 (one per new step) in the direction of signal decrease and increase, the dependence is divided into sections. These sections have different sizes, because the data points separated by intervals In_1 are differently located between the minimum and the maximum values. Actions on one large initial step St_1 end when the edges of the interval reach the minimum and maximum.
6. Approximation of the dependence of the total noise on the signal level at each interval according to the equation:

$$\sigma\,(x) = \sqrt{a^2x^2 + bx + c^2} \tag{10}$$

where x is the signal, a is an approximation of the PRNU value, b is an approximation of the gain K and c is an approximation of the dark noise:

$$\mathrm{c} = \sqrt{\sigma_{dt}^2 + DSNU^2} \tag{11}$$

   a. Approximation of the dependence of temporal noise on the signal level at each interval according to the equation:

$$\sigma_t\,(x) = \sqrt{b_1x + c_1^2} \tag{12}$$

   b. Approximation of the spatial noise dependence on the signal level according to the equation:

$$\sigma_s\,(x) = \sqrt{a_1^2x^2 + c_2^2} \tag{13}$$

   c. Parameters $a1$ and $b1$ are used as initial values of the a and b, respectively. The smallest of c_1 and c_2 is the initial value of parameter c. Next, the dependence of the total noise on the signal level is approximated using such values as initial ones.
7. Forming arrays of *PRNU*, K and *dark noise* estimates obtained from approximations over all intervals of In_1 and In_2. At the same time, arrays of interval lengths and standard deviations (STDs) corresponding to each of these noise estimates are formed. STD is calculated between two dependencies that were estimated using the interval analysis and using the whole range of signals.
8. Calculation of weighting factors for *PRNU*, K, and d*ark noise*. The weighting strategy is based on two fundamental assumptions:

a. The larger the signal interval used for approximation, the more reliable the estimate, since it is supported by a greater number of samples. Extremely small intervals may not contain sufficient statistical information and therefore should not dominate the final result. Such intervals are interpreted as local corrective adjustments rather than primary contributors.
b. Noise parameters of modern digital cameras lie within relatively stable practical ranges. Estimates that strongly deviate from these ranges are more likely to arise from local distortions of the noise–signal dependency. Therefore, the weighting mechanism moderately reduces the influence of such outlying estimates while still retaining them to avoid artificial truncation of valid but rare cases.

Thus, the weights can be interpreted as composite confidence indicators combining statistical support and physical consistency.

Each of the weighting factors has two coefficients. The first coefficient is common for all 3 noise parameters. It is calculated as the ratio of two values: the normalized interval value and normalized STD value for this estimation. The interval value is normalized to the size of the considered data set (noises and averages), to which the considered estimation corresponds. The STD value is normalized to the maximum of all STDs obtained on all intervals of the In_1 and In_2. The second coefficient was calculated on the basis of experimental observations of the internal statistics of the *PRNU*, K, and *dark noise* estimation arrays:

a. Weighting coefficient for PRNU.
The PRNU magnitude is typically on the order of 10^{-3} [39], as confirmed by experimental observations [42]. The weight for PRNU is calculated as the modulus of the normalized difference of the decimal logarithms of PRNU (for a given interval) and 10^{-3} normalized to the maximum modulus of the difference of these quantities over all intervals In_1 and In_2. Calculation through the logarithm was chosen because it is convenient to represent PRNU as 10^{-n} in order of magnitude. To ensure the necessary correct distribution of weights, the obtained values are subtracted from 1:

$$W_{PRNU}(i,j) = \left|1 - \left|\frac{\left|log_{10}(PRNU(i,j))\right| - \left|log_{10}(0.001)\right|}{MAX(Norm_{PRNU})}\right|\right|$$
$$Norm_{PRNU} = \left|\left|log_{10}(PRNU(i,j))\right| - \left|log_{10}(0.001)\right|\right| \quad (14)$$

where *PRNU(i,j)* is the array of PRNU estimates, *(i,j)* are the number of columns and rows of the *PRNU(i,j)* array.
PRNU value using nonuniform frames were estimated in [75]. However, the frames had low non-uniformity (less than 20%), and PRNU value was estimated from multiple images. Therefore, an additional novelty of our work is the first time PRNU value estimation from a single nonuniform image.

b. Weighting coefficient for K.
The estimate of the gain K is in many cases [42] close to those obtained by more accurate methods. The weight for gain K is calculated as the modulus of the difference between two values: the median value for all intervals of In_1 and In_2 and the one under consideration. The obtained value is normalized to the maximum modulus of the difference of these values at all intervals In_1 and In_2. To ensure the correct distribution of weights, the obtained values are subtracted from 1:

$$W_K(i,j) = \left|1 - \left|\frac{K(i,j) - median(K(i,j))}{MAX(Norm_K)}\right|\right|$$
$$Norm_K = |K(i,j) - median(K(i,j))| \quad (15)$$

where *K(i,j)* is the array of estimates of the gain conversion K, *median(K(i,j))* is the median value for the array of estimates *K(i,j)*, *(i, j)* are the number of columns and rows of the array *K(i,j)*.

c. Weighting coefficient for the dark noise.
Usually there are few pixels on the image that can be used for dark noise estimation. This is due to the fact that regions with very dark signals are rare in a random image. Only special scenes (e.g., strongly gradient [44], [45] or strip [47]) can have both dark and light regions. Therefore, the weight for dark noise was calculated depending on the number of close dark noise estimates obtained. The fewer the number of neighboring dark noise estimates within a tolerance range, the greater the assigned weight:

$$W_{dark}(i,j) = \left|1 - \frac{Num(i,j)}{N \times M}\right|$$
$$Num(i,j) = \sum_{k=1}^{N}\sum_{l=1}^{M} \begin{cases} 1, & if\ round\ (Dark(i,j) - Dark(k,l)) = 0 \\ 0, & if\ round\ (Dark(i,j) - Dark(k,l)) \neq 0 \end{cases} \quad (16)$$

where N, M – number of columns and rows of the dark noise array *Dark(i, j)*, *round* – rounding operator to the nearest integer, *Dark(i, j)* – array of coefficients of dark noise estimates, *(i, j)* and *(k, l)* – row and column numbers of the *Dark(i, j)*.

Due to the dependence of the weight on interval size and stability, a small number of narrow intervals cannot dominate the final estimate under normal operating conditions. Only intervals that simultaneously

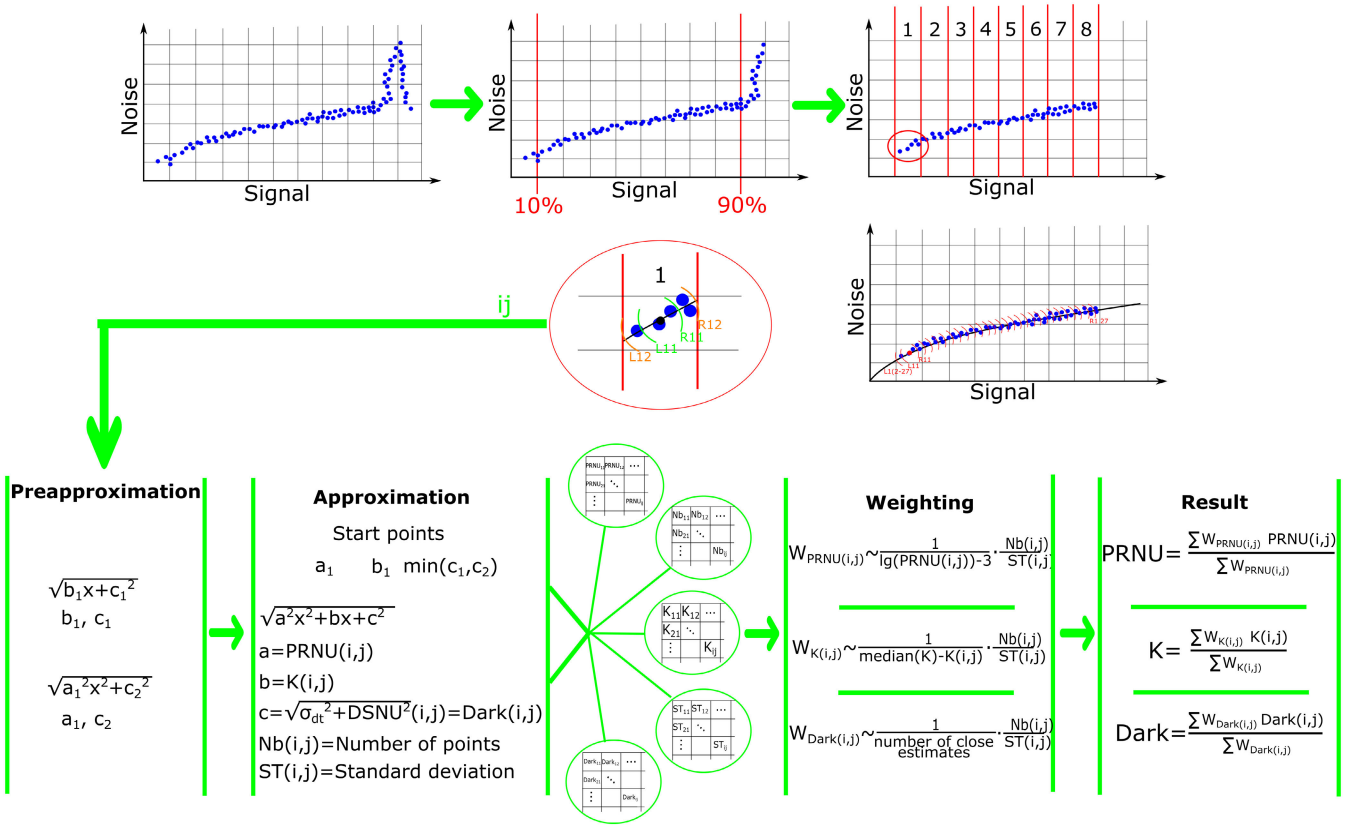

FIGURE 3. Main steps of the proposed method for noise estimation from a single image.

provide sufficient statistical support and physically consistent parameter values obtain substantial influence in the final aggregation. In particular, intervals with larger signal spans inherently receive higher weights because they contain more samples and therefore yield more stable regression estimates, whereas narrow intervals are treated as local refinements with reduced influence. In parallel, estimates that deviate significantly from the median or from physically plausible ranges are down-weighted through normalization procedures, ensuring that anomalous values contribute only marginally to the final aggregation. The chosen segmentation parameters ensure that each interval contains a sufficient number of samples for stable regression while preserving sensitivity to local deviations. Moderate variation of these parameters does not significantly affect the final weighted estimates.

9. Obtaining the final estimates of light and dark noise using the weighted averaging:

$$PRNU = \frac{\sum W_{PRNU}(i,j)\, PRNU(i,j)}{\sum W_{PRNU}(i,j)} \tag{17}$$

$$K = \frac{\sum W_{K}(i,j)\, K(i,j)}{\sum W_{K}(i,j)} \tag{18}$$

$$Dark = \frac{\sum W_{dark}(i,j)\, Dark(i,j)}{\sum W_{dark}(i,j)} \tag{19}$$

The main steps of the proposed method for noise estimation from a single image are shown in Fig. 3.

The proposed method allows for more efficient approximation than the standard approaches for the following reasons:

1. The experimentally obtained points are divided into multiple sections. In result the amount of input data is increased and thereby small sections can be taken into account.
2. When considering multiple sections, a statistical method can be used. This method is weighted averaging with a well-founded construction of weighting coefficients.
3. Weighted averaging allows for effective use of a priori information about the noise characteristics of digital camera sensors.

IV. EXPERIMENTAL VERIFICATION OF THE METHOD

A. NOISE VS SIGNAL DEPENDENCY ESTIMATION

The proposed method was verified on the real images. To validate the proposed modification described in Section III-A (1st stage of the method), we registered images by consumer mirrorless camera Canon EOS M100 (CMOS sensor, 6000×4000 pixels, $3.7 \times 3.7 \mu$m pixel size). The images from the dataset (dataset of consumer images, DCI) can be found in [96]. The measured by the Standard EMVA 1288 noises of the camera [42] are presented in Table 1. Since the camera uses a colour sensor, only pixels corresponding to one colour

TABLE 1. Measured by the standard parameters.

Parameter	Value
PRNU, relative units	0.0092±0.0003
DSNU, DN	0.191±0.005
K, DN/e	0.781±0.006
σdt, DN	2.479±0.004

channel were used. Linear unprocessed images were obtained in standard graphical format using a dcraw converter [97].

Examples of the registered images for the methods testing are shown in Fig. 4: shots of amateur (Fig. 4a,b,c), nonuniform (Fig. 4g), uniform (Fig. 4h) and strip scene (Fig. 4j). Firstly, the modified method O. Laligant was applied to the images. This is the 1st stage of the main proposed method. The obtained dependencies of total noise on signal level are shown in Fig. 4d-f, k-m. For comparison, the dependencies obtained by the EMVA 1288 Standard were shown also.

For nonuniform (Fig. 4g) and uniform scenes (Fig. 4h), the estimated dependencies closely match the EMVA reference curves (Fig. 4k-l). The dependencies (Fig. 4d-e) for the amateur images in Fig. 4a-b provide satisfactory degree of similarity with the Standard. For the amateur image in Fig. 4c the method overestimates the noise in the first half of the plot and underestimates in the second half (Fig. 4f).

The quality of the obtained dependency visually indicates whether reliable parameter extraction is possible. Strong deviation from smooth square-root behavior or limited dynamic-range coverage signals insufficient suitability of the input image for EMVA-based decomposition.

Therefore, for reliable noise estimation, images with smooth nonuniform gradients are preferable. An example of an available method of obtaining a nonuniform image in an amateur environment is sunset recording.

To evaluate the robustness of the proposed weighting scheme, a dataset consisting of 361 raw images acquired under varying illumination conditions, ISO settings, aperture values, and exposure times was analyzed (Canon EOS M100, 6000 × 4000 pixels). For each image, the full set of interval weights used in the final averaging procedure was extracted and statistically evaluated. The relative dispersion of interval weights with respect to their mean value was calculated. Across the entire dataset, the average dispersion was approximately 25%. This observation demonstrates that larger and statistically stable intervals receive greater weights, confirming that the method differentiates between more and less reliable approximations. The moderate dispersion indicates that no small subset of intervals systematically dominates the final estimates. The contribution remains distributed across multiple segments of the noise–signal dependency.

B. APPROXIMATION OF THE PATCH-BASED OBTAINED DEPENDENCIES

The patch-based approximation considered here corresponds conceptually to classical Poisson–Gaussian noise fitting approaches [73], which estimate signal-dependent variance but do not perform explicit EMVA component separation. Therefore, this experiment serves as a representative baseline for single-image composite-noise estimation methods.

The modified method O. Laligant provides noise vs signal dependency. This is 1st stage of the main proposed method of the noise estimation. To demonstrate the method possibilities, we firstly evaluated noise characteristics by direct approximation of the dependencies. The direct approximation consists of 3 stages:

1. Application of proposed modification of the O. Laligant patch-based method.
2. Readout of the signal array and deviation array from the noise vs signal dependency.
3. Approximation of values by the function that has the form $\sqrt{a^2x^2 + bx + c^2}$, i.e. it corresponds to (10).

Since this algorithm is based on the data from the modified O. Laligant method, it is patch-based approximation.

The obtained estimates are shown in Table 2. Percentage deviations from the values measured with the Standard are also given. In the Section IV-C these results will be compared with the main proposed method.

It can be seen that it is practically impossible to obtain a correct estimation of light spatial and dark noise when using the patch-based approximation. The estimation error is often hundreds of percent. The conversion gain K estimates in most cases coincide in order of magnitude with the Standard ones. However, for this parameter one can see both cases of significant error and acceptable accuracy. The highest estimation accuracy is achieved when using nonuniform images.

Thus, we can conclude that in order to obtain adequate noise estimates by single-image methods, it is necessary to use as nonuniform frames with smooth gradients as possible.

C. NOISE ESTIMATION BY THE PROPOSED METHOD

The dependencies in Fig. 4 are the 1st stage of the main method of the digital camera noise characteristics estimation. Using these plots, we evaluated noises by the method (see Section IV). The obtained estimates are shown in Table 3. Percentage deviations from the values measured with the Standard are also given.

Table 3 shows that in the majority of cases the noise estimation errors had been reduced from hundreds of percent (see Table 2) to tens and even units. The proposed method failed 2 times only, which is indicated by dashes in the Table 3.

To evaluate robustness with respect to signal interval selection, various truncation configurations were tested: 10–90% (baseline), 1–99% (extended), and 20–80% (restricted mid-range). The results show that the proposed method remains stable under moderate threshold variations, and the qualitative conclusions remain unchanged. When the interval is extended to 1–99%, parameter dispersion increases slightly. This effect is caused by inclusion of boundary regions: low-signal regions are affected by quantization noise and residual offsets, while near-saturation areas may violate

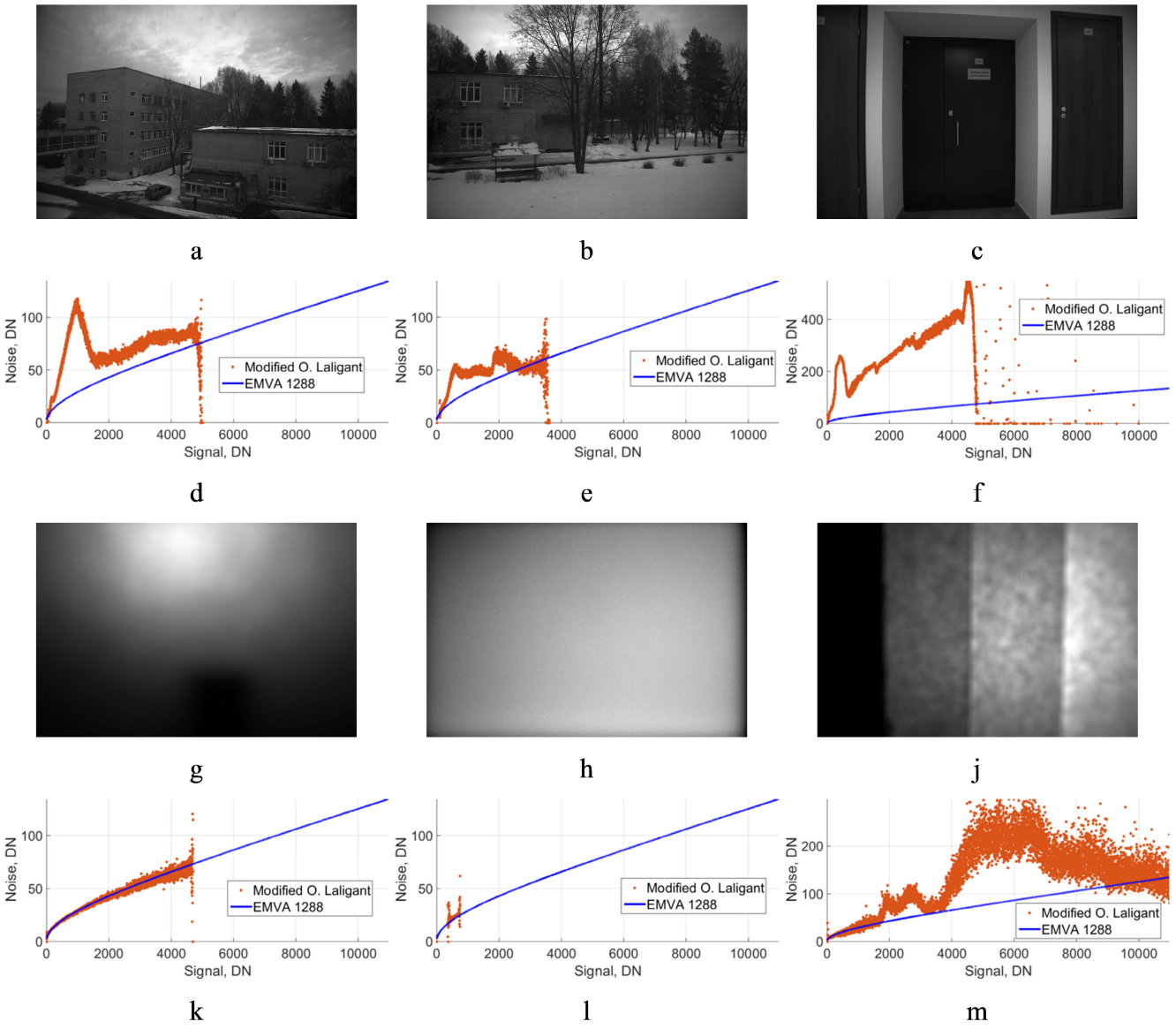

FIGURE 4. Images of amateur (a-c), non-uniform (g), uniform (h) and strip (j) scenes and the corresponding dependencies (below the images: d-f, k, l and m) of total noise on signal level.

linear response assumptions. Restricting the interval to 20–80% improves numerical stability and reduces variability across images. However, the reduced dynamic span decreases slope sensitivity, which may slightly increase uncertainty of the gain estimate when signal variation is limited. These observations indicate a bias–variance trade-off in truncation selection: wider intervals increase information content but introduce boundary sensitivity, whereas narrower intervals improve robustness at the cost of reduced dynamic leverage.

V. DISCUSSION

To analyze the results and identify the most effective methods for noise estimation from a single image, we estimated the average error for different types of images. The information is presented in Table 4. Percentage deviations from the values measured with the Standard are also given.

In order to demonstrate the results in a convenient form, we made diagrams. They are summarized in Fig. 5. The accuracy of noise estimation is presented. For each type of scene, the point on the diagram corresponds to a value from the worst (at the center circle) to the best (at the outer circle).Therefore, the larger the area of the green heptagon, the better and more accurate the method performs. Results are shown for two cases of frames: the most popular common (amateur) images and the most suitable nonuniform scenes. If the dot is located on the outer circle, the noise estimation is fully consistent with the EMVA 1288 Standard measurements. If the point is located on the inner circle, the difference of noise estimation from the Standard is 100% or more. The further from the center the number of failures is located, the fewer errors occurred in the process of experimental testing of the method and, therefore, the more reliable it is.

TABLE 2. Noise estimation by patch-based approximation.

Image type	Value PRNU, rel.un.	Deviation from the Standard value, %
Amateur 1	$3.7 \cdot 10^{-5}$	99.6
Amateur 2	$2.2 \cdot 10^{-7}$	100
Amateur 3	0.23	2400
Nonuniform	0.088	860
Uniform	0.0087	5.8
Strip	$7.3 \cdot 10^{-4}$	92
Image type	Gain K, DN/e	
Amateur 1	0.93	19
Amateur 2	1.0	28
Amateur 3	26	3300
Nonuniform	0.78	0.4
Uniform	1.0	34
Strip	3.4	330
Image type	Dark noise, DN	
Amateur 1	52	2000
Amateur 2	23	840
Amateur 3	0.032	99
Nonuniform	0.010	99.6
Uniform	0.012	99.5
Strip	0.014	99.4

TABLE 3. Noise estimation by the proposed method.

Image type	Value PRNU, rel.un.	Deviation from the Standard value, %
Amateur 1	0.0064	31
Amateur 2	0.0091	1.1
Amateur 3	0.010	8.4
Nonuniform	—	
Uniform	0.0084	8.3
Strip	0.0094	2.5
Image type	Gain K, DN/e	
Amateur 1	0.27	65
Amateur 2	0.44	44
Amateur 3	0.15	81
Nonuniform	0.75	3.3
Uniform	0.57	27
Strip	0.39	50
Image type	Dark noise, DN	
Amateur 1	4.3	74
Amateur 2	2.9	16
Amateur 3	—	
Nonuniform	0.27	89
Uniform	6.5	160
Strip	0.85	66

TABLE 4. Mean noise estimates error for the proposed method.

Image type	Amateur images	Special images	All images
	PRNU, relative units		
Absolute deviation	0.0012	0.0005	0.0009
Relative deviation, %	13	5.4	10
	K, DN/e		
Absolute deviation	0.50	0.21	0.35
Relative deviation, %	63	27	45
	Dark noise, DN		
Absolute deviation	1.1	2.6	2.0
Relative deviation, %	45	106	81

Thus, the proposed method is promising for amateur-level camera noise estimation. It can be seen that the method can be applied to various images. The special prepared images provide better noise parameter accuracy. Even random amateur images yield errors on the order of tens of percent, which was previously unattainable using single-image approaches.

Nonuniform images provide the best accuracy among considered object types. Such an image can be realized extremely easily. For example, you can take images of sunset or the gradient zones of the surrounding world. Another example is making shots when the part of the radiation directed to the camera sensor is blocked. In this case image includes both light and dark areas.

The proposed method is very fast compared to the standard measurements. The camera noises are estimated by the proposed method using a single image only. The standard requires registering about a hundred of images of dozens scenes.

The overall accuracy of the method is primarily determined by the correctness of the estimated noise–signal dependency at the first stage. When this dependency is consistent with the physical Poisson–Gaussian model, the multi-interval approximation and weighted averaging effectively suppress local deviations and reduce estimation variance. However, if the input image contains strong structural heterogeneity that violates the assumptions of the initial estimation algorithm, the resulting dependency may be biased, leading to inaccurate EMVA parameter extraction. In such cases, the limitation is associated mainly with the initial single-image noise estimation stage rather than with the proposed decomposition framework.

Although the proposed method improves robustness through segmentation and weighted averaging, reliable estimation requires that the initial noise–signal dependency satisfies several conditions. Failure cases may occur under the following conditions:

1. If strong structural variations dominate local statistics, the single-image noise estimation stage may produce a

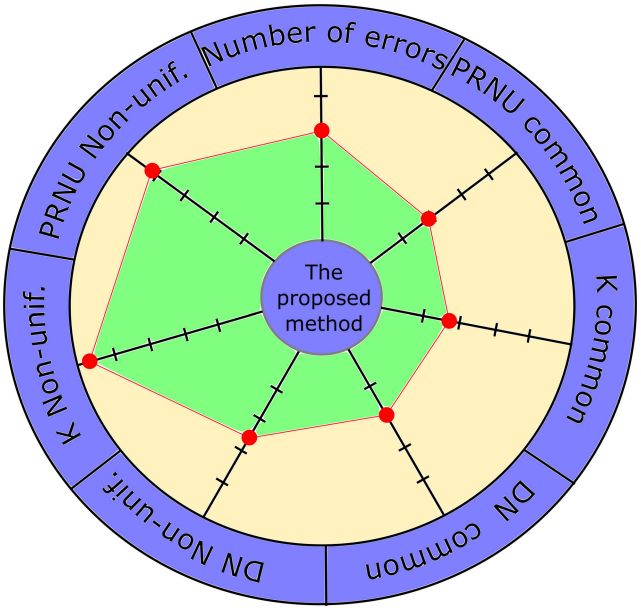

FIGURE 5. Performance of the proposed method for a single nonuniform and common (amateur) images. Quality of PRNU, gain K and dark noise DN estimation and number of failures (errors) are analysed. The larger the area of the green heptagon is, the more accurate the proposed method works.

distorted dependency. In this case, the deviation curve does not reflect sensor noise but residual scene structure.

2. Small image sizes or limited signal diversity reduce the number of samples available per interval, leading to unstable approximations and increased variance of the estimated parameters.
3. The EMVA-based decomposition assumes square-root dependence of temporal noise on signal level. If the empirical curve strongly deviates from this model (e.g., due to saturation, nonlinear processing, rolling shutter effects, or internal camera corrections), reliable separation of components becomes problematic.

Highly textured scenes, sharp edges, extreme low-light conditions and partial saturation or nonlinear camera processing can lead to violation of the Poisson-Gaussian noise approximation. Therefore, to ensure applicability of the method, the goodness-of-fit of the square-root approximation (e.g., normalized residual error or coefficient of determination R^2) should be evaluated. A low fitting quality indicates that the image does not satisfy the assumptions required for reliable parameter extraction. At the same time wide dynamic range generally improves estimation reliability, as it provides broader signal coverage and increased statistical support for approximation.

Future work includes validation on additional camera types (both CCD and CMOS) as well as systematic sensitivity analysis and formal determination of optimal heuristic parameters. Another direction of further investigation is verification of the method on initial data that were obtained by other ideas. A systematic comparison with representative filtering-, wavelet-, and deep learning–based single-image noise estimation methods, combined with adaptation of their outputs to EMVA 1288 parameters, is part of our ongoing research. Such comparison requires reformulating composite noise estimates into physically interpretable sensor parameters, which is beyond the scope of the present validation-focused study. The current work should therefore be considered as methodological approbation of the proposed EMVA-oriented decomposition framework.

VI. CONCLUSION

For the first time, a method for accurate estimation of digital camera noise parameters from a single image is proposed. The method uses segmentation and multi-parameter analysis of signal deviation dependencies on the signal level. It can estimate light spatial noise, PRNU value, light temporal noise, and dark noise separately.

The proposed method was experimentally verified. It yields a significant increase in noise estimation accuracy compared to even patch-based data approximation. The noise estimation error is reduced from hundreds of percent to units and several tens of percent.

The method is a very promising and can be applied to various images. Nonuniform images provide the best accuracy. Additionally, the method is significantly faster than measurements performed according to the standard.

The method can statistically separate light noise of different types from each other and from dark noise, which can be useful in a number of image processing tasks, including noise reduction, pattern recognition, and camera identification.

REFERENCES

[1] J. Suo, W. Zhang, J. Gong, X. Yuan, D. J. Brady, and Q. Dai, "Computational imaging and artificial intelligence: The next revolution of mobile vision," *Proc. IEEE*, vol. 111, no. 12, pp. 1607–1639, Dec. 2023, doi: 10.1109/JPROC.2023.3338272.

[2] S. E. Salcudean, H. Moradi, D. G. Black, and N. Navab, "Robot-assisted medical imaging: A review," *Proc. IEEE*, vol. 110, no. 7, pp. 951–967, Jul. 2022, doi: 10.1109/JPROC.2022.3162840.

[3] R. Chengoden, N. Victor, T. Huynh-The, G. Yenduri, R. H. Jhaveri, M. Alazab, S. Bhattacharya, P. Hegde, P. K. R. Maddikunta, and T. R. Gadekallu, "Metaverse for healthcare: A survey on potential applications, challenges and future directions," *IEEE Access*, vol. 11, pp. 12765–12795, 2023, doi: 10.1109/ACCESS.2023.3241628.

[4] D. T. Swain, I. D. Couzin, and N. Ehrich Leonard, "Real-time feedback-controlled robotic fish for behavioral experiments with fish schools," *Proc. IEEE*, vol. 100, no. 1, pp. 150–163, Jan. 2012, doi: 10.1109/JPROC.2011.2165449.

[5] L. J. Nowak and M. Lankheet, "Fish detection using electrical impedance spectroscopy," *IEEE Sensors J.*, vol. 22, no. 21, pp. 20855–20865, Nov. 2022, doi: 10.1109/JSEN.2022.3207921.

[6] C. Huang, Y. Hou, W. Ye, D. Huang, X. Huang, B. Lin, and D. Cai, "NeRF-Det++: Incorporating semantic cues and perspective-aware depth supervision for indoor multi-view 3D detection," *IEEE Trans. Image Process.*, vol. 34, pp. 2575–2587, 2025, doi: 10.1109/TIP.2025.3560240.

[7] Y. Wu, R. Li, Z. Qin, X. Zhao, and X. Li, "HeightFormer: Explicit height modeling without extra data for camera-only 3D object detection in bird's eye view," *IEEE Trans. Image Process.*, vol. 34, pp. 689–700, 2025, doi: 10.1109/TIP.2024.3427701.

[8] F. Sippel, J. Seiler, and A. Kaup, "Multispectral snapshot image registration using learned cross spectral disparity estimation and a deep guided occlusion reconstruction network," *IEEE Trans. Image Process.*, vol. 34, pp. 2338–2350, 2025, doi: 10.1109/TIP.2025.3556602.

[9] G. Dwivedi, L. Pensia, V. Lohchab, and R. Kumar, "Nondestructive inspection and quantification of soldering defects in PCB using an autofocusing digital holographic camera," *IEEE Trans. Instrum. Meas.*, vol. 72, pp. 1–8, 2023, doi: 10.1109/TIM.2023.3298390.

[10] Y. Chen, Z. Fan, Z. Chen, and Y. Zhu, "CA-Jaccard: Camera-aware Jaccard distance for person re-identification," in *Proc. IEEE/CVF Conf. Comput. Vis. Pattern Recognit. (CVPR)*, Jun. 2024, pp. 17532–17541, doi: 10.1109/CVPR52733.2024.01660.

[11] K. Uemura, K. Kiyokawa, and N. Sakata, "End-to-end gaze estimation method for surveillance camera images," *IEEE Access*, vol. 13, pp. 182276–182285, 2025, doi: 10.1109/ACCESS.2025.3621428.

[12] T. Fischer, T. E. Huang, J. Pang, L. Qiu, H. Chen, T. Darrell, and F. Yu, "QDTrack: Quasi-dense similarity learning for appearance-only multiple object tracking," *IEEE Trans. Pattern Anal. Mach. Intell.*, vol. 45, no. 12, pp. 15380–15393, Dec. 2023, doi: 10.1109/TPAMI.2023.3301975.

[13] M. Adl, R. Ahmed, C. Vidal, and A. Emadi, "Enhanced vehicle movement counting at intersections via a self-learning fisheye camera system," *IEEE Access*, vol. 12, pp. 77947–77958, 2024, doi: 10.1109/ACCESS.2024.3408052.

[14] Y. Fan, J. Li, Y. Guo, L. Xie, and G. Zhang, "Digital image colorimetry on smartphone for chemical analysis: A review," *Measurement*, vol. 171, Feb. 2021, Art. no. 108829, doi: 10.1016/j.measurement.2020.108829.

[15] M. R. I. Udoy, S. Alam, M. M. Islam, A. Jaiswal, and A. Aziz, "A review of digital pixel sensors," *IEEE Access*, vol. 13, pp. 8533–8551, 2025, doi: 10.1109/ACCESS.2025.3526879.

[16] O. Burggraaff, N. Schmidt, J. Zamorano, K. Pauly, S. Pascual, C. Tapia, E. Spyrakos, and F. Snik, "Standardized spectral and radiometric calibration of consumer cameras," *Opt. Exp.*, vol. 27, no. 14, p. 19075, Jun. 2019, doi: 10.1364/oe.27.019075.

[17] A. Pandharipande, C.-H. Cheng, J. Dauwels, S. Z. Gurbuz, J. Ibanez-Guzman, G. Li, A. Piazzoni, P. Wang, and A. Santra, "Sensing and machine learning for automotive perception: A review," *IEEE Sensors J.*, vol. 23, no. 11, pp. 11097–11115, Jun. 2023, doi: 10.1109/JSEN.2023.3262134.

[18] Y. Chi, X. Zhang, and S. H. Chan, "HDR imaging with spatially varying signal-to-noise ratios," in *Proc. IEEE/CVF Conf. Comput. Vis. Pattern Recognit. (CVPR)*, Jun. 2023, pp. 5724–5734, doi: 10.1109/CVPR52729.2023.00554.

[19] S. Friday, Y. Shi, Y. Cherivirala, V. Saragadam, and A. Pediredla, "Snapshot LiDAR: Fourier embedding of amplitude and phase for single-image depth reconstruction," in *Proc. IEEE/CVF Conf. Comput. Vis. Pattern Recognit. (CVPR)*, Jun. 2024, pp. 25203–25212, doi: 10.1109/CVPR52733.2024.02381.

[20] C. F. Andersen, I. Farup, and J. Y. Hardeberg, "Additivity constrained linearisation of camera calibration data," *IEEE Trans. Image Process.*, vol. 32, pp. 3774–3789, 2023, doi: 10.1109/TIP.2023.3287735.

[21] P. J. Withagen, F. C. A. Groen, and K. Schutte, "CCD color camera characterization for image measurements," *IEEE Trans. Instrum. Meas.*, vol. 56, no. 1, pp. 199–203, Feb. 2007, doi: 10.1109/TIM.2006.887667.

[22] I. Lee, B. Kim, and H. Joo, "Guess the unseen: Dynamic 3D scene reconstruction from partial 2D glimpses," in *Proc. IEEE/CVF Conf. Comput. Vis. Pattern Recognit. (CVPR)*, Jun. 2024, pp. 1062–1071, doi: 10.1109/CVPR52733.2024.00107.

[23] R. Manekar, E. Negrini, M. Pham, D. Jacobs, J. Srivastava, S. J. Osher, and J. Miao, "Low-light phase retrieval with implicit generative priors," *IEEE Trans. Image Process.*, vol. 33, pp. 4728–4737, 2024, doi: 10.1109/TIP.2024.3445739.

[24] M. Maggioni, E. Sánchez-Monge, and A. Foi, "Joint removal of random and fixed-pattern noise through spatiotemporal video filtering," *IEEE Trans. Image Process.*, vol. 23, no. 10, pp. 4282–4296, Oct. 2014, doi: 10.1109/TIP.2014.2345261.

[25] K. Zhang, S. Kulshrestha, and C. A. Metzler, "A scalable training strategy for blind multi-distribution noise removal," *IEEE Trans. Image Process.*, vol. 33, pp. 6216–6226, 2024, doi: 10.1109/TIP.2024.3482185.

[26] S. Herbreteau and C. Kervrann, "Linear combinations of patches are unreasonably effective for single-image denoising," *IEEE Trans. Image Process.*, vol. 33, pp. 4600–4613, 2024, doi: 10.1109/TIP.2024.3436651.

[27] W. Meiniel, J.-C. Olivo-Marin, and E. D. Angelini, "Denoising of microscopy images: A review of the state-of-the-art, and a new sparsity-based method," *IEEE Trans. Image Process.*, vol. 27, no. 8, pp. 3842–3856, Aug. 2018, doi: 10.1109/TIP.2018.2819821.

[28] K. Dabov, A. Foi, V. Katkovnik, and K. Egiazarian, "Image denoising by sparse 3-D transform-domain collaborative filtering," *IEEE Trans. Image Process.*, vol. 16, no. 8, pp. 2080–2095, Aug. 2007, doi: 10.1109/TIP.2007.901238.

[29] M. Georgiev, R. Bregovic, and A. Gotchev, "Fixed-pattern noise modeling and removal in time-of-flight sensing," *IEEE Trans. Instrum. Meas.*, vol. 65, no. 4, pp. 808–820, Apr. 2016, doi: 10.1109/TIM.2015.2494622.

[30] N. Li, B. Wang, F. Goudail, Y. Zhao, and Q. Pan, "Joint denoising-demosaicking network for long-wave infrared division-of-focal-plane polarization images with mixed noise level estimation," *IEEE Trans. Image Process.*, vol. 32, pp. 5961–5976, 2023, doi: 10.1109/TIP.2023.3327590.

[31] Y. Cao, M. Liu, S. Liu, X. Wang, L. Lei, and W. Zuo, "Physics-guided ISO-dependent sensor noise modeling for extreme low-light photography," in *Proc. IEEE/CVF Conf. Comput. Vis. Pattern Recognit. (CVPR)*, Jun. 2023, pp. 5744–5753, doi: 10.1109/CVPR52729.2023.00556.

[32] Y. Zou, Y. Fu, Y. Zhang, T. Zhang, C. Yan, and R. Timofte, "Calibration-free raw image denoising via fine-grained noise estimation," *IEEE Trans. Pattern Anal. Mach. Intell.*, vol. 47, no. 7, pp. 5368–5384, Jul. 2025, doi: 10.1109/TPAMI.2025.3550264.

[33] B. Henz, E. S. L. Gastal, and M. M. Oliveira, "Synthesizing camera noise using generative adversarial networks," *IEEE Trans. Vis. Comput. Graphics*, vol. 27, no. 3, pp. 2123–2135, Mar. 2021, doi: 10.1109/TVCG.2020.3012120.

[34] Z. Dang, M. Luo, J. Wang, C. Jia, H. Han, H. Wan, G. Dai, X. Chang, and J. Wang, "Disentangled noisy correspondence learning," *IEEE Trans. Image Process.*, vol. 34, pp. 2602–2615, 2025, doi: 10.1109/TIP.2025.3559457.

[35] M. Ghulyani and M. Arigovindan, "Fast roughness minimizing image restoration under mixed Poisson–Gaussian noise," *IEEE Trans. Image Process.*, vol. 30, pp. 134–149, 2021, doi: 10.1109/TIP.2020.3032036.

[36] E. Onzon, F. Mannan, and F. Heide, "Neural auto-exposure for high-dynamic range object detection," in *Proc. IEEE/CVF Conf. Comput. Vis. Pattern Recognit. (CVPR)*, Jun. 2021, pp. 7706–7716, doi: 10.1109/CVPR46437.2021.00762.

[37] N. Moran, D. Schmidt, Y. Zhong, and P. Coady, "Noisier2Noise: Learning to denoise from unpaired noisy data," in *Proc. IEEE/CVF Conf. Comput. Vis. Pattern Recognit. (CVPR)*, Jun. 2020, pp. 12061–12069, doi: 10.1109/CVPR42600.2020.01208.

[38] Q. Wen, S. Zhu, S. Liu, H. Guo, J. Jin, and Y. Zhu, "Image sensor correction algorithm for photon transfer curve based on neural network," *Opt. Eng.*, vol. 59, no. 6, p. 1, Jun. 2020, doi: 10.1117/1.oe.59.6.067102.

[39] (2016). *EMVA Standard 1288, Standard for Characterization of Image Sensors and Cameras*. [Online]. Available: https://www.emva.org/standards-technology/emva-1288/emva-standard-1288-downloads-2/

[40] J. Nakamura, *Image Sensors and Signal Processing for Digital Still Cameras*. London, U.K.: Informa, 2005, doi: 10.1201/9781420026856.

[41] E. Gastasini, N. Capecci, F. Lupi, A. Gagliardi, S. Saponara, and M. Lanzetta, "An instrument for the characterization and calibration of optical sensors," *Sensors*, vol. 21, no. 15, p. 5141, Jul. 2021, doi: 10.3390/s21155141.

[42] A. V. Kozlov, V. G. Rodin, R. S. Starikov, N. N. Evtikhiev, and P. A. Cheremkhin, "A family of methods based on automatic segmentation for estimating digital camera noise: A review," *IEEE Sensors J.*, vol. 24, no. 11, pp. 17353–17365, Jun. 2024, doi: 10.1109/JSEN.2024.3390418.

[43] A. V. Kozlov, V. G. Rodin, R. S. Starikov, N. N. Evtikhiev, and P. A. Cheremkhin, "Estimation of camera's noise by uniform target segmentation," *IEEE Sensors J.*, vol. 23, no. 5, pp. 4883–4891, Mar. 2023, doi: 10.1109/JSEN.2023.3238673.

[44] A. Foi, S. Alenius, V. Katkovnik, and K. Egiazarian, "Noise measurement for raw-data of digital imaging sensors by automatic segmentation of nonuniform targets," *IEEE Sensors J.*, vol. 7, no. 10, pp. 1456–1461, Oct. 2007, doi: 10.1109/JSEN.2007.904864.

[45] P. A. Cheremkhin, N. N. Evtikhiev, V. V. Krasnov, V. G. Rodin, and S. N. Starikov, "Modified temporal noise measurement method with automatic segmentation of nonuniform target, its accuracy estimation, and application to cameras of different types," *Opt. Eng.*, vol. 53, no. 10, Jul. 2014, Art. no. 102107, doi: 10.1117/1.oe.53.10.102107.

[46] A. Foi, M. Trimeche, V. Katkovnik, and K. Egiazarian, "Practical Poissonian-Gaussian noise modeling and fitting for single-image raw-data," *IEEE Trans. Image Process.*, vol. 17, no. 10, pp. 1737–1754, Oct. 2008, doi: 10.1109/TIP.2008.2001399.

[47] N. N. Evtikhiev, A. V. Kozlov, V. V. Krasnov, V. G. Rodin, R. S. Starikov, and P. A. Cheremkhin, "A method for measuring digital camera noise by automatic segmentation of a striped target," *Comput. Opt.*, vol. 45, no. 2, pp. 267–276, Apr. 2021, doi: 10.18287/2412-6179-co-815.

[48] V. A. Pimpalkhute, R. Page, A. Kothari, K. M. Bhurchandi, and V. M. Kamble, "Digital image noise estimation using DWT coefficients," *IEEE Trans. Image Process.*, vol. 30, pp. 1962–1972, 2021, doi: 10.1109/TIP.2021.3049961.

[49] X. Liu, M. Tanaka, and M. Okutomi, "Practical signal-dependent noise parameter estimation from a single noisy image," *IEEE Trans. Image Process.*, vol. 23, no. 10, pp. 4361–4371, Oct. 2014, doi: 10.1109/TIP.2014.2347204.

[50] O. Laligant, F. Truchetet, and E. Fauvet, "Noise estimation from digital step-model signal," *IEEE Trans. Image Process.*, vol. 22, no. 12, pp. 5158–5167, Dec. 2013, doi: 10.1109/TIP.2013.2282123.

[51] C. Liu, R. Szeliski, S. Bing Kang, C. L. Zitnick, and W. T. Freeman, "Automatic estimation and removal of noise from a single image," *IEEE Trans. Pattern Anal. Mach. Intell.*, vol. 30, no. 2, pp. 299–314, Feb. 2008, doi: 10.1109/TPAMI.2007.1176.

[52] S.-C. Tai and S.-M. Yang, "A fast method for image noise estimation using Laplacian operator and adaptive edge detection," in *Proc. 3rd Int. Symp. Commun., Control Signal Process.*, Mar. 2008, pp. 1077–1081, doi: 10.1109/isccsp.2008.4537384.

[53] Y. Zhang, G. Wang, and J. Xu, "Parameter estimation of signal-dependent random noise in CMOS/CCD image sensor based on numerical characteristic of mixed Poisson noise samples," *Sensors*, vol. 18, no. 7, p. 2276, Jul. 2018, doi: 10.3390/s18072276.

[54] T. Hai Thai, F. Retraint, and R. Cogranne, "Generalized signal-dependent noise model and parameter estimation for natural images," *Signal Process.*, vol. 114, pp. 164–170, Sep. 2015, doi: 10.1016/j.sigpro.2015.02.020.

[55] S.-M. Yang, "Fast and reliable image-noise estimation using a hybrid approach," *J. Electron. Imag.*, vol. 19, no. 3, Jul. 2010, Art. no. 033007, doi: 10.1117/1.3476329.

[56] A. De Stefano, P. R. White, and W. B. Collis, "Training methods for image noise level estimation on wavelet components," *EURASIP J. Adv. Signal Process.*, vol. 2004, no. 16, Dec. 2004, Art. no. 405209, doi: 10.1155/s1110865704401218.

[57] M. Hashemi and S. Beheshti, "Adaptive noise variance estimation in BayesShrink," *IEEE Signal Process. Lett.*, vol. 17, no. 1, pp. 12–15, Jan. 2010, doi: 10.1109/LSP.2009.2030856.

[58] X. Liu, M. Tanaka, and M. Okutomi, "Single-image noise level estimation for blind denoising," *IEEE Trans. Image Process.*, vol. 22, no. 12, pp. 5226–5237, Dec. 2013, doi: 10.1109/TIP.2013.2283400.

[59] S. Pyatykh, J. Hesser, and L. Zheng, "Image noise level estimation by principal component analysis," *IEEE Trans. Image Process.*, vol. 22, no. 2, pp. 687–699, Feb. 2013, doi: 10.1109/TIP.2012.2221728.

[60] J. Li, Y. Wu, Y. Zhang, J. Zhao, and Y. Si, "Parameter estimation of Poisson–Gaussian signal-dependent noise from single image of CMOS/CCD image sensor using local binary cyclic jumping," *Sensors*, vol. 21, no. 24, p. 8330, Dec. 2021, doi: 10.3390/s21248330.

[61] G. Chen, F. Zhu, and P. A. Heng, "An efficient statistical method for image noise level estimation," in *Proc. IEEE Int. Conf. Comput. Vis. (ICCV)*, Santiago, Chile, Dec. 2015, pp. 477–485, doi: 10.1109/ICCV.2015.62.

[62] L. Dong, J. Zhou, and Y. Y. Tang, "Effective and fast estimation for image sensor noise via constrained weighted least squares," *IEEE Trans. Image Process.*, vol. 27, no. 6, pp. 2715–2730, Jun. 2018, doi: 10.1109/TIP.2018.2812083.

[63] D.-H. Shin, R.-H. Park, S. Yang, and J.-H. Jung, "Block-based noise estimation using adaptive Gaussian filtering," *IEEE Trans. Consum. Electron.*, vol. 51, no. 1, pp. 218–226, Feb. 2005, doi: 10.1109/TCE.2005.1405723.

[64] F. Li, F. Fang, Z. Li, and T. Zeng, "Single image noise level estimation by artificial noise," *Signal Process.*, vol. 213, Dec. 2023, Art. no. 109215, doi: 10.1016/j.sigpro.2023.109215.

[65] H. Chen, J. Gu, Y. Liu, S. A. Magid, C. Dong, Q. Wang, H. Pfister, and L. Zhu, "Masked image training for generalizable deep image denoising," in *Proc. IEEE/CVF Conf. Comput. Vis. Pattern Recognit. (CVPR)*, Vancouver, BC, Canada, Jun. 2023, pp. 1692–1703, doi: 10.1109/CVPR52729.2023.00169.

[66] H. Tan, H. Xiao, S. Lai, Y. Liu, and M. Zhang, "Pixelwise estimation of signal-dependent image noise using deep residual learning," *Comput. Intell. Neurosci.*, vol. 2019, pp. 1–12, Sep. 2019, doi: 10.1155/2019/4970508.

[67] R. Ma, Y. Zhang, B. Zhang, L. Fang, D. Huang, and L. Qi, "Learning attention in the frequency domain for flexible real photograph denoising," *IEEE Trans. Image Process.*, vol. 33, pp. 3707–3721, 2024, doi: 10.1109/TIP.2024.3404253.

[68] Y. Zou and Y. Fu, "Estimating fine-grained noise model via contrastive learning," in *Proc. IEEE/CVF Conf. Comput. Vis. Pattern Recognit. (CVPR)*, Jun. 2022, pp. 12672–12681, doi: 10.1109/CVPR52688.2022.01235.

[69] J. Byun, S. Cha, and T. Moon, "FBI-denoiser: Fast blind image denoiser for Poisson–Gaussian noise," in *Proc. IEEE/CVF Conf. Comput. Vis. Pattern Recognit. (CVPR)*, Jun. 2021, pp. 5764–5773, doi: 10.1109/CVPR46437.2021.00571.

[70] Y. Huang and H. Huang, "Beyond image prior: Embedding noise prior into latent space of conditional denoising transformer," *Int. J. Comput. Vis.*, vol. 133, no. 11, pp. 7591–7611, Aug. 2025, doi: 10.1007/s11263-025-02553-w.

[71] M. Wischow, P. Irmisch, A. Boerner, and G. Gallego, "Real-time noise source estimation of a camera system from an image and metadata," *Adv. Intell. Syst.*, vol. 6, no. 6, Apr. 2024, Art. no. 2300479, doi: 10.1002/aisy.202300479.

[72] Y. Luo, L. Fu, N. Jia, T. Wang, R. Li, and B. Zhang, "MSR-Net: A novel noise elimination method for real CMOS image sensor," *IEEE Access*, vol. 12, pp. 78714–78725, 2024, doi: 10.1109/ACCESS.2024.3407966.

[73] A. A. Volkov, A. V. Kozlov, P. A. Cheremkhin, D. A. Rymov, A. V. Shifrina, R. S. Starikov, V. A. Nebavskiy, E. K. Petrova, E. Y. Zlokazov, and V. G. Rodin, "A review of neural network-based image noise processing methods," *Sensors*, vol. 25, no. 19, p. 6088, Oct. 2025, doi: 10.3390/s25196088.

[74] K. Wei, Y. Fu, Y. Zheng, and J. Yang, "Physics-based noise modeling for extreme low-light photography," *IEEE Trans. Pattern Anal. Mach. Intell.*, vol. 44, no. 11, pp. 8520–8537, Nov. 2022, doi: 10.1109/TPAMI.2021.3103114.

[75] Y. Wang, B. Wan, G. Fu, and Y. Su, "PRNU estimation of linear CMOS image sensors that allows nonuniform illumination," *IEEE Trans. Instrum. Meas.*, vol. 70, pp. 1–11, 2021, doi: 10.1109/TIM.2021.3088484.

[76] D. Martin, C. Fowlkes, D. Tal, and J. Malik, "A database of human segmented natural images and its application to evaluating segmentation algorithms and measuring ecological statistics," in *Proc. 8th IEEE Int. Conf. Comput. Vis.*, Oct. 2001, pp. 416–423, doi: 10.1109/ICCV.2001.937655.

[77] L. Zhang. *McMaster Image Dataset*. Accessed: Dec. 25, 2025. [Online]. Available: https://www4.comp.polyu.edu.hk/{~}cslzhang/CDM_Dataset.htm

[78] (2025). *The USC-SIPI Image Database*. [Online]. Available: https://sipi.usc.edu/database/

[79] A. Abdelhamed, S. Lin, and M. S. Brown, "A high-quality denoising dataset for smartphone cameras," in *Proc. IEEE/CVF Conf. Comput. Vis. Pattern Recognit.*, Jun. 2018, pp. 1692–1700, doi: 10.1109/CVPR.2018.00182.

[80] T. Plötz and S. Roth, "Benchmarking denoising algorithms with real photographs," in *Proc. IEEE Conf. Comput. Vis. Pattern Recognit. (CVPR)*, Jul. 2017, pp. 2750–2759, doi: 10.1109/CVPR.2017.294.

[81] M. L. Uss, B. Vozel, V. V. Lukin, and K. Chehdi, "Image informative maps for component-wise estimating parameters of signal-dependent noise," *J. Electron. Imag.*, vol. 22, no. 1, Feb. 2013, Art. no. 013019, doi: 10.1117/1.jei.22.1.013019.

[82] B. Jähne. (1288). *Simulated Camera Data for EMVA 1288 Verification*. Accessed: Oct. 1, 2025. [Online]. Available: https://hci.iwr.uni-heidelberg.de/Simulated_Camera_Data_for_EMVA_1288_Verification

[83] *GitHub-EMVA1288/Datasets*. Accessed: Dec. 25, 2025. [Online]. Available: https://github.com/EMVA1288/datasets

[84] H. Maitre, *From Photon to Pixel: The Digital Camera Handbook*. Hoboken, NJ, USA: Wiley, 2015.

[85] K. Nakamoto and H. Hotaka, "Efficient and accurate conversion-gain estimation of a photon-counting image sensor based on the maximum likelihood estimation," *Opt. Exp.*, vol. 30, no. 21, p. 37493, Sep. 2022, doi: 10.1364/oe.471394.

[86] W. R. Bennett, "Spectra of quantized signals," *Bell Syst. Tech. J.*, vol. 27, no. 3, pp. 446–472, Jul. 1948, doi: 10.1002/j.1538-7305.1948.tb01340.x.

[87] V. D. Silva, V. Chesnokov, and D. Larkin, "A novel adaptive shading correction algorithm for camera systems," *Electron. Imag.*, vol. 28, no. 18, pp. 1–5, Feb. 2016, doi: 10.2352/issn.2470-1173.2016.18.dpmi-249.

[88] B. L. Preece and D. P. Haefner, "3D noise photon transfer curve," *Appl. Opt.*, vol. 61, no. 21, p. 6202, Jul. 2022, doi: 10.1364/ao.452166.

[89] S. W. Zamir, A. Arora, S. Khan, M. Hayat, F. S. Khan, M.-H. Yang, and L. Shao, "CycleISP: Real image restoration via improved data synthesis," in *Proc. IEEE/CVF Conf. Comput. Vis. Pattern Recognit. (CVPR)*, Seattle, WA, USA, Jun. 2020, pp. 2693–2702, doi: 10.1109/CVPR42600.2020.00277.
[90] S. W. Zamir, A. Arora, S. Khan, M. Hayat, F. S. Khan, M.-H. Yang, and L. Shao, "Multi-stage progressive image restoration," in *Proc. IEEE/CVF Conf. Comput. Vis. Pattern Recognit. (CVPR)*, Nashville, TN, USA, Jun. 2021, pp. 14816–14826, doi: 10.1109/CVPR46437.2021.01458.
[91] K. He, X. Zhang, S. Ren, and J. Sun, "Deep residual learning for image recognition," in *Proc. IEEE Conf. Comput. Vis. Pattern Recognit. (CVPR)*, Las Vegas, NV, USA, Jun. 2016, pp. 770–778, doi: 10.1109/CVPR.2016.90.
[92] S. W. Zamir, A. Arora, S. Khan, M. Hayat, F. S. Khan, and M. Yang, "Restormer: Efficient transformer for high-resolution image restoration," in *Proc. IEEE/CVF Conf. Comput. Vis. Pattern Recognit. (CVPR)*, Jun. 2022, pp. 5718–5729, doi: 10.1109/CVPR52688.2022.00564.
[93] M. Mäkitalo and A. Foi, "Noise parameter mismatch in variance stabilization, with an application to Poisson–Gaussian noise estimation," *IEEE Trans. Image Process.*, vol. 23, no. 12, pp. 5348–5359, Dec. 2014, doi: 10.1109/TIP.2014.2363735.
[94] H. Yue, C. Cao, L. Liao, R. Chu, and J. Yang, "Supervised raw video denoising with a benchmark dataset on dynamic scenes," in *Proc. IEEE/CVF Conf. Comput. Vis. Pattern Recognit. (CVPR)*, Jun. 2020, pp. 2298–2307, doi: 10.1109/CVPR42600.2020.00237.
[95] Y. Wang, H. Huang, Q. Xu, J. Liu, Y. Liu, and J. Wang, "Practical deep raw image denoising on mobile devices," in *Proc. ECCV*, Aug. 2020, pp. 1–16, doi: 10.1007/978-3-030-58539-6_1.
[96] *Dataset-Consumer-Images (DCI)*. Accessed: Apr. 2, 2026. [Online]. Available: https://github.com/k1121/Dataset-consumer-images
[97] D. Coffin. *Decoding Raw Digital Photos in Linux*. Accessed: Apr. 2, 2026. [Online]. Available: https://www.dechifro.org/dcraw/

ALEXANDER V. KOZLOV received the M.S. degree in laser technologies and the Ph.D. degree in laser physics from National Research Nuclear University MEPhI (Moscow Engineering Physics Institute), Moscow, Russia, in 2021 and 2025, respectively.

Since 2019, he has been an Engineer with MEPhI. His research interests include digital holography, noise modeling, and digital image processing.

PAVEL A. CHEREMKHIN received the M.A. degree in solid-state physics and nanosystems, the Ph.D. degree in laser physics, and the D.Sc. degree in optics from National Research Nuclear University MEPhI (Moscow Engineering Physics Institute), Moscow, Russia, in 2010, 2013, and 2025, respectively.

Since 2016, he has been a Researcher and an Associate Professor with the Laser Physics Department, MEPhI. He has co-authored more than 50 journal articles and more than 60 conference proceedings. His research interests include holography, digital image processing, deep learning, and camera characterization.

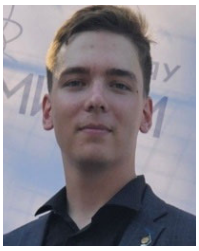

ANTON A. VOLKOV received the B.S. degree in laser technologies from National Research Nuclear University MEPhI (Moscow Engineering Physics Institute), Moscow, Russia, in 2024, where he is currently pursuing the M.S. degree in laser technologies.

Since 2022, he has been an Engineer with MEPhI. His research interests include deep learning, digital image processing, and camera characterization.

ANDREY S. SVISTUNOV received the M.S. degree in laser technologies from National Research Nuclear University MEPhI (Moscow Engineering Physics Institute), Moscow, Russia, in 2024, where he is currently pursuing the Ph.D. degree in laser physics.

Since 2023, he has been an Engineer with MEPhI. His research interests include digital holography, deep learning, and digital image processing.

ROSTISLAV S. STARIKOV received the M.A. degree in optical equipment and systems from Russian Technological University (RTU MIREA), in 1993, and the Ph.D. degree in laser physics and the D.Sc. degree in optoelectronic information processing from National Research Nuclear University MEPhI (Moscow Engineering Physics Institute), Moscow, Russia, in 1997 and 2011, respectively.

Since 2012, he has been a Professor with the Laser Physics Department, MEPhI. He has co-authored more than 50 journal articles and more than 60 conference proceedings. His research interests include laser physics, information optics, and microwave photonics.

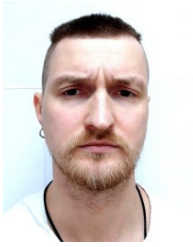

VSEVOLOD A. NEBAVSKIY received the M.S. degree in laser technologies and the Ph.D. degree in laser physics from National Research Nuclear University MEPhI (Moscow Engineering Physics Institute), Moscow, Russia, in 2018 and 2024, respectively.

Since 2025, he has been an Associate Professor with the Laser Physics Department, MEPhI. He has co-authored more than ten journal articles. His research interests include microwave photonics, laser physics, and information optics.

EVGENII YU. ZLOKAZOV received the M.A. degree in solid-state physics and the Ph.D. and D.Sc. degrees in laser physics from National Research Nuclear University MEPhI (Moscow Engineering Physics Institute), Moscow, Russia, in 2006, 2011, and 2021, respectively.

Since 2022, he has been a Professor with the Laser Physics Department, MEPhI. He has co-authored more than 30 journal articles and more than 50 conference proceedings. His research interests include information optics, laser physics, and microwave photonics.

VLADISLAV G. RODIN received the M.A. degree in solid-state physics, the Ph.D. degree in laser physics, and the D.Sc. degree in optics from National Research Nuclear University MEPhI (Moscow Engineering Physics Institute), Moscow, Russia, in 1989, 1999, and 2022, respectively.

Since 2024, he has been a Leading Researcher with the Laser Physics Department, MEPhI. He has co-authored more than 40 journal articles and more than 50 conference proceedings. His research interests include holography, optical image processing, and diffraction optics.